Science of the Total Environment 885 (2023) 163711

Contents lists available at ScienceDirect

Science of the Total Environment

journal homepage: www.elsevier.com/locate/scitotenv

Do we need high temporal resolution modelling of exposure in urban areas? A test case

H. Woodward [a,*], A. Schroeder [b], A. de Nazelle [a], C.C. Pain [c], M.E.J. Stettler [d], H. ApSimon [a], A. Robins [e], P.F. Linden [f]

[a] Centre for Environmental Policy, Imperial College London, London, UK
[b] MRC Epidemiology Unit, University of Cambridge School of Clinical Medicine, Clifford Allbutt Building, Cambridge Biomedical Campus, Cambridge, UK
[c] Department of Earth Science and Engineering, Imperial College London, London, UK
[d] Centre for Transport Studies, Faculty of Engineering, Department of Civil and Environmental Engineering, Imperial College London, London, UK
[e] Department of Mechanical Engineering Sciences, University of Surrey, Guildford, UK
[f] Department of Applied Mathematics and Theoretical Physics, Centre for Mathematical Sciences, University of Cambridge, Cambridge, UK

HIGHLIGHTS

- Exposures are resolved down to the time scale of the breathing cycling (1 s).
- High temporal resolution needed to accurately derive distribution of 1 s exposures.
- Exposure is characterised by low concentrations punctuated by short duration peaks.
- Proximity and timing of emission peaks important in determining mean exposure
- Avoiding largest peaks could significantly reduce mean exposure.

GRAPHICAL ABSTRACT

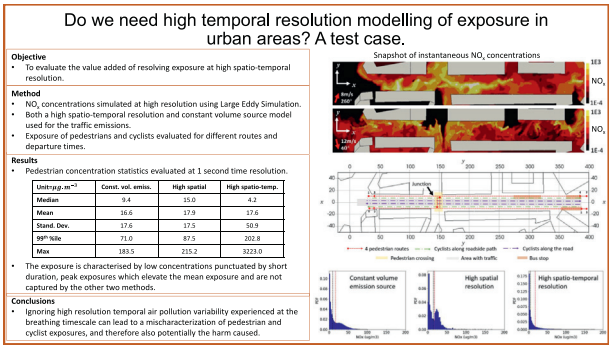

ARTICLE INFO

Editor: Pavlos Kassomenos

Keywords:
Air pollution
Exposure
High resolution
Modelling
Road transport
NOx

ABSTRACT

Roadside concentrations of harmful pollutants such as NO_x are highly variable in both space and time. This is rarely considered when assessing pedestrian and cyclist exposures.

We aim to fully describe the spatio-temporal variability of exposures of pedestrians and cyclists travelling along a road at high resolution. We evaluate the value added of high spatio-temporal resolution compared to high spatial resolution only. We also compare high resolution vehicle emissions modelling to using a constant volume source. We highlight conditions of peak exposures, and discuss implications for health impact assessments.

Using the large eddy simulation code Fluidity we simulate NO_x concentrations at a resolution of 2 m and 1 s along a 350 m road segment in a complex real-world street geometry including an intersection and bus stops. We then simulate pedestrian and cyclist journeys for different routes and departure times.

For the high spatio-temporal method, the standard deviation in 1 s concentration experienced by pedestrians (50.9 μg.m^{-3}) is nearly three times greater than that predicted by the high-spatial only (17.5 μg.m^{-3}) or constant volume source (17.6 μg.m^{-3}) methods. This exposure is characterised by low concentrations punctuated by short duration, peak exposures which elevate the mean exposure and are not captured by the other two methods. We also find that the mean exposure of cyclists on the road (31.8 μg.m^{-3}) is significantly greater than that of cyclists on a roadside path (25.6 μg.m^{-3}) and that of pedestrians on a sidewalk (17.6 μg.m^{-3}).

We conclude that ignoring high resolution temporal air pollution variability experienced at the breathing time scale can lead to a mischaracterization of pedestrian and cyclist exposures, and therefore also potentially the harm caused. High resolution methods reveal that peaks, and hence mean exposures, can be meaningfully reduced by avoiding hyper-local hotspots such as bus stops and junctions.

* Corresponding author.
E-mail address: huw.woodward@imperial.ac.uk (H. Woodward).

http://dx.doi.org/10.1016/j.scitotenv.2023.163711
Received 22 December 2022; Received in revised form 10 April 2023; Accepted 20 April 2023
Available online 4 May 2023

1. Introduction

Air quality models help us to understand the nature of exposure to harmful pollutants. This includes the location and cause of elevated concentrations within urban areas, source apportionment and the quantification of exposure within different micro-environments (e.g. different travelling modes). As methods have become more advanced and computer power has increased, many models have increased their spatial resolution with exposure analyses now possible down to the scale of metres (e.g. Santiago et al., 2022; Beevers et al., 2012). For population exposure estimates, Santiago et al. (2022) used high resolution modelling (down to ~1 m) of a city in Spain to demonstrate that a grid resolution of 1 km^2 or finer is required in order to generate accurate population-level statistics such as total population exposure. These models are also useful for identifying key local hotspots within the city, for example at busy junctions (Santiago et al., 2021), which contribute to the short term variability in exposure of individuals. Santiago et al. (2021) (Santiago et al., 2021) used their high-resolution concentration maps, along with pedestrian mobility microsimulations to calculate pedestrian exposure. They found that the high-resolution spatial mapping picked up concentration hotspots at busy junctions, leading to an increase in the estimate of total exposure by 9–23 %, compared with a spatially averaged approach. While there is a recognition that it is important to understand the variation in concentrations within urban areas at high spatial resolution, the same cannot be said for high temporal resolution modelling. This is despite the well-known variability in vehicle emissions, which tend to be dominated by very short peaks associated with transient periods of high engine load, e.g. when accelerating from standstill or changing gear (O'Driscoll et al., 2016; Irwin et al., 2018). Measurements have shown that these peaks constitute the vast majority of the total emitted NO_x during real world driving (Peckham et al., 2020), yet the correlation between the location and timing of these peak emissions with pedestrian and cyclist movement is not well understood.

When modelling down to scales of metres, the associated time scales for concentration fluctuations is in the order of seconds. Yet, high spatial resolution models of pollutant concentrations tend to consider 1 h mean concentrations, neglecting any fluctuations in concentration within these hourly periods. Of course, estimating the exposure of individuals as they move through these high spatial resolution maps leads to variations in exposure with time, at time scales of seconds, e.g. as pedestrians walk through hotspots with length scales of a few metres they experience elevated concentrations for a few seconds. Santiago et al. (2021) showed that this variation leads to a log-normal distribution in exposures across the 300 m × 300 m area that they simulated. However, when considered at the level of an individual, these modelled short time scale variations are in fact entirely artificial, as the actual concentration experienced at any particular time or location can, for a majority of the time, diverge significantly from the time-averaged mean. In order to capture the full variation in exposures about the mean it is necessary to resolve concentrations at time scales down to that of the breathing cycle, i.e. to the order of 1 s for active travel. Further, ignoring the variation in concentrations with time at high resolution also risks missing potentially significant effects such as the coupling of the time periods during which pedestrians stand waiting to cross at the roadside with the time period during which vehicle emissions are greatest, i.e. pedestrians are required to wait at the roadside edge while vehicles accelerate past generating high emissions, but are able to walk without delay during the period at which vehicles are stationary and emissions are at their lowest. Similarly, cyclists who ride on the road are often forced to stop at traffic lights among polluting vehicles, often within a metre or two from the nearest tailpipe. At these distances the concentrations to which a cyclist is exposed is likely to be significantly greater than the time-average mean, albeit for only a short period of time. These occurrences and their contribution to total exposure are not fully captured by lower time resolution models, regardless of the spatial resolution used.

In this paper we use the high spatio-temporal resolution simulations of NO_x concentrations along a road in London, as presented by Woodward et al. (2022), to quantify the exposure of pedestrians and cyclists as they travel along the road. The simulations are used to investigate to what extent the exposure of pedestrians and cyclists quantified at 1 s resolution differs from that quantified using a high spatial but low temporal resolution representation of concentrations. A comparison is also made with the exposure to traffic emissions modelled as a constant volume source spanning the length of the street. In addition to the mean exposure of the pedestrians and cyclists we also consider the variation in exposures about the mean for each exposure calculation method. The potential significance of this variation is then discussed, drawing on a toxicokinetic toxicodynamic model of harm (Rozman and Doull, 2000; Rozman, 2000) to illustrate why the variation in exposure over short time periods may be significant when evaluating the impact on health.

2. Methodology

The modelling used to simulate the exposure of pedestrians and cyclists along the road consists of four elements:

1. The vehicles moving along the road.
2. The second-by-second emissions of each vehicle.
3. The dispersion of the traffic tailpipe emissions.
4. The movement of pedestrians and cyclists as they travel along the road and their resulting exposure to traffic emissions.

A detailed description of the methods used for steps 1 to 3 is given in Woodward et al. (2022), however we also provide a summary here, followed by a description of the method used for step 4. The flow chart shown in Fig. 1 shows each step of the methodology and the inputs required. In this paper we focus on step 4.

2.1. High resolution modelling of NO_x concentrations

Fluidity is an open-source software developed at Imperial College London. It is a general purpose, finite element computational fluid dynamics software within which a large eddy simulation (LES) methodology is implemented with an anisotropic adaptive mesh (Pain et al., 2001). Using LES, Fluidity is able to simulate unsteady atmospheric flows, resolving turbulent features of the flow and the dispersion of passive tracers down to length and time scales of <1 m and < 1 s, respectively (Woodward et al., 2019; Aristodemou et al., 2018; Pavlidis et al., 2010). Fig. 2 shows the buildings included in the model and a snapshot of the velocity magnitude on a plane crossing London road, where turbulent features of the flow can be seen. The full geometry domain used for the simulation had dimensions 1000 m × 850 m × 300 m.

Emissions from vehicle tailpipes were modelled using two methods. The first represented the emissions as a constant volume source extending the length and width of the road (the grey area in Fig. 3). The second represented the emissions as volume sources with time-varying emission rates. These sources have a minimum size of 2 m × 2 m × 2 m and move along the street. The length of a volume source along the direction of travel of the vehicle increases as the vehicle speed increases,

ensuring a smooth, continuous source between simulation time steps as described in Woodward et al. (2022).

The emission rate of each individual vehicle is calculated using an instantaneous NO_x emissions model (Le Cornec et al., 2020) and the vehicle movement is modelled using the PTV Vissim traffic flow model (PTV Vissim, n.d.), providing a reasonable representation of real-world driving behaviour, including response to traffic light signals. Combination of the instantaneous emissions model with Fluidity's high resolution airflow calculations allows the dispersion of tailpipe emissions to be modelled at high spatial and temporal resolution. Fluidity's ability to replicate realistic concentration variations at the roadside is demonstrated in Woodward et al. (2022).

Only the NO_x emissions from the tailpipes of vehicles travelling down the road, named London Road, are modelled and analysed in this paper. No assumption is made for other sources or background NO_x concentration.

Four runs were used for the analysis, each simulating 45 min of the dispersion of traffic emission along the road. These comprised of two wind speeds and directions and two different configurations of the traffic light timings at the junction at $x \approx 150$ m (see Fig. 3). They are summarised in Table 1. For both meteorological conditions, the atmospheric boundary layer was assumed to be neutral (i.e. wind driven with mechanical mixing dominant) and applied using a Synthetic Eddy Method (Pavlidis et al., 2010). The prevailing wind speeds and directions at 200 m were chosen to replicate measurements taken during two periods of a field study at London Road, while the profile of the mean wind speed and turbulence was scaled up from a wind tunnel model of the site (see Woodward et al., 2022 for more detail). While the wind speeds and directions were a crude replication of two periods of the field study, it should be noted that evaluating the model performance at the high time resolution considered here is very difficult, and the comparison made in Woodward et al. (2022) is far from perfect, for example it was not possible to exactly replicate the meteorological conditions and traffic flows of the field study. Despite this, in Woodward et al. (2022) we demonstrate that the method is able to replicate similar statistics to the measurements. Additional meteorological conditions can be considered in future.

Fig. 4 shows two examples of the instantaneous NO_x concentration field at two random times during the simulations. The concentrations are seen to vary by orders of magnitude within the street, reaching as high as 1000 μg. m^{-3} in small areas. The blue arrows indicate the direction of street level dispersion due to the street canyon effect within the street, which changes for the two wind directions considered.

In order to minimise the demand on hard disk space and memory, the concentrations calculated by Fluidity for each time step were saved only on a 2 m × 2 m grid along the entire length and width of the road at a height of 1 m, rather than for all of the computational nodes within the street, which numbered in the millions. Concentrations were generated at each time step, either 0.25 s or 0.33 s, but were reduced to 1 s time resolution by averaging over 1 s periods for the duration of the simulation. This was to reduce computational demand when running the exposure analysis. The length and time scales used for the exposure analysis described here are therefore 2 m and 1 s, respectively.

2.2. Pedestrian and cyclist exposures

The pedestrian and cyclist exposures were calculated using a Python script to interrogate the Fluidity concentration output files. The routes travelled by the pedestrians and cyclists along a roadside path were programmed within this script, using simplifying assumptions such as straight line trajectories and constant moving speeds. The routes for the cyclists travelling along the road were simulated as part of the PTV simulations which generated the vehicle trajectories. In this case it was important to capture the interaction between vehicles and cyclists.

2.2.1. Pedestrian routes

Four routes were defined for pedestrians to walk along the road in either direction, as shown in Fig. 3. A total of 200 pedestrians were sent along each route at intervals of 10 s. Each pedestrian walked in a perfectly straight line at 1.3 ms^{-1} until they reached the junction at approximately $x =$

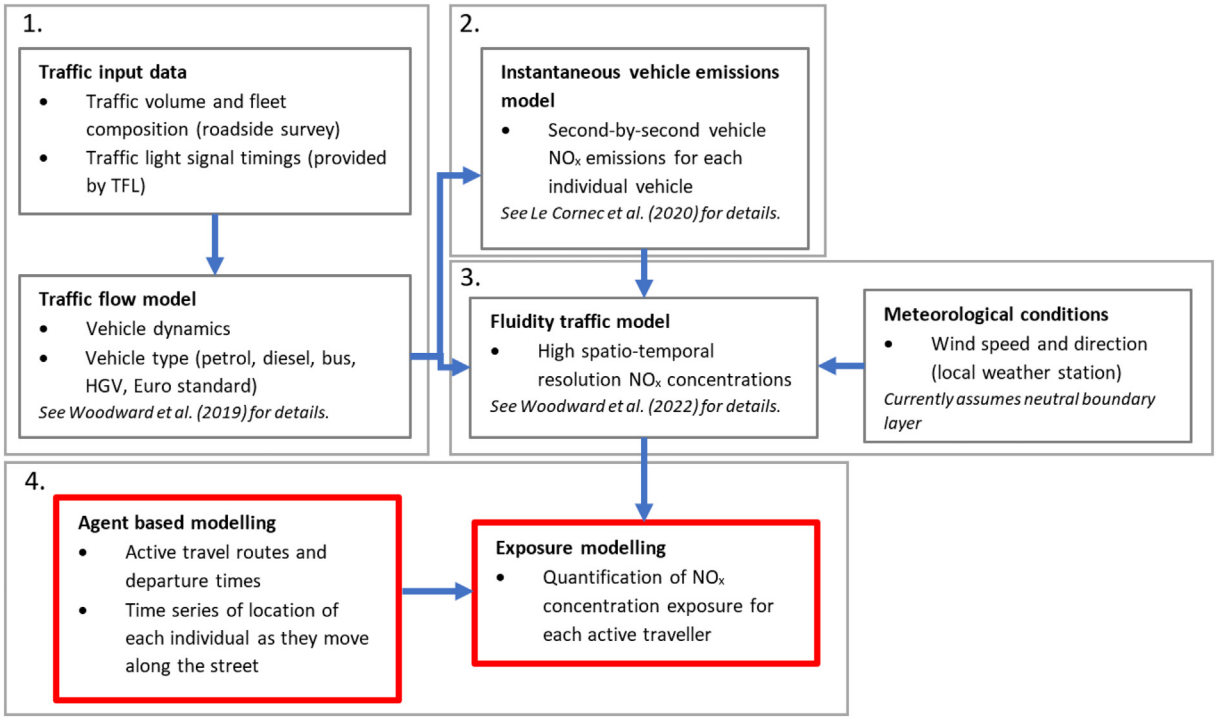

Fig. 1. Flow chart of methodology used to simulate high spatio-temporal exposure of pedestrians and cyclists to NO_x concentrations from traffic emissions. Details of the methodology for the grey boxes can be found in Woodward et al. (2022) and in the papers referenced. TFL denotes Transport for London.

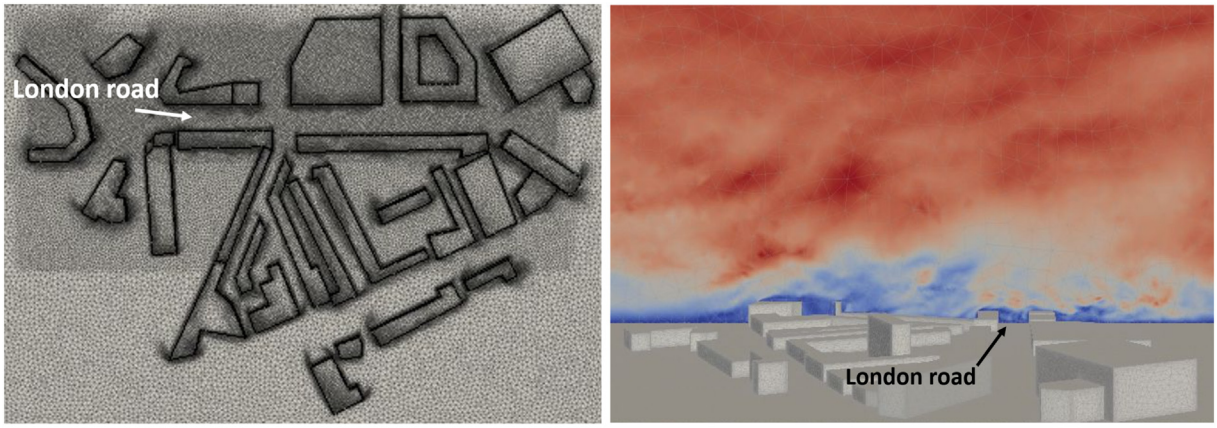

Fig. 2. (a) Modelled street geometry and (b) a snapshot of the wind velocity magnitude across the geometry perpendicular to London Road. The full geometry domain used for the simulation had dimensions 1000 m × 850 m × 300 m.

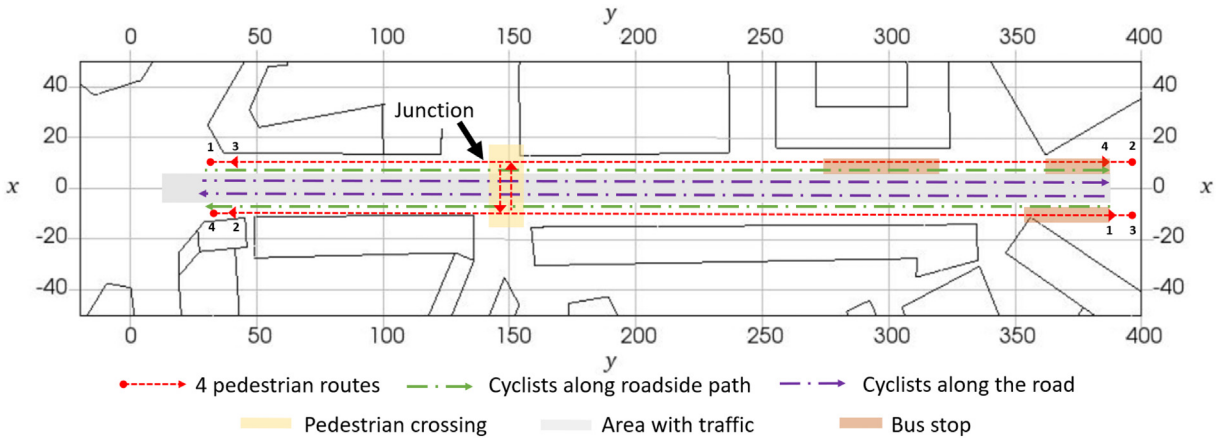

Fig. 3. Routes taken by pedestrians and cyclists along London Road.

150 m. Once at the junction the pedestrians crossed if the vehicles had been stopped by the traffic lights. Otherwise, pedestrians waited at the roadside until that occurred before continuing along their route. A scatter was introduced in the location at which the pedestrians stopped and waited at the roadside such that each pedestrian did not occupy the exact same location each time. This scatter was defined somewhat arbitrarily, as were the routes taken by pedestrians. Changing these parameters would lead to a change in calculated exposures, however the objective of this work is to demonstrate the utility of high resolution modelling, rather than a comprehensive study of pedestrian exposures along London Road - this is a case study varying only a limited range of parameters and the results should be considered within this context. The mean journey time for the pedestrians was 317 s, with a standard deviation of 21 s.

Table 1
Meteorology and traffic light configuration for the four simulation runs, and the number of vehicles, pedestrians and cyclists per hour. u_{ref} denotes the wind speed at the reference height of 200 m.

Run	u_{ref} ms^{-1}	Wind dir.	Traffic light cycle	N veh./h	N Ped.	N Cyc. (P)	N Cyc. (R)
1	8	260°	48 s	874	800	800	79
2	12	40°	48 s	874	800	800	79
3	8	260°	96 s	833	800	800	67
4	12	40°	96 s	833	800	800	67

Cyc.(P) denotes cyclists travelling on a roadside cycle path. Cyc.(R) denotes cyclists travelling on the road.

2.2.2. Cyclists routes along a roadside path

The exposure of cyclists travelling along the road was calculated using two separate methods. The first used a similar method to that for the pedestrians and is referred to as cyclists(P). Two straight line routes were defined for the cyclists; one along the edge of the road in either direction. For each route, 200 cyclists at 10 s intervals travelled at a constant speed of 5 ms^{-1} unless stopped at the junction by red lights. These cyclists stopped ahead of the waiting vehicles and did not respond or interact in any way with the vehicles. For example, if approaching a queue of vehicles at the traffic lights, these cyclists continued to travel at 5 ms^{-1} until they reached their stopping point ahead of the vehicles. In this way this first group of cyclists were not required at any time to wait directly behind any vehicles. The mean and standard deviation of journey time of the cyclists was 80 s and 10 s, respectively.

2.2.3. Cyclists routes along the road

The second group of cyclists was simulated by the PTV Vissim microsimulation model and travelled along the road itself. These are referred to as cyclists(R). These travelled along the road with the vehicles and stopped at any red lights with the vehicles before continuing once the signal turned green. No effort was made to move past stationary vehicles ahead of the cyclists, therefore when approaching a queue at the traffic lights these cyclists waited directly behind the vehicle ahead; representing

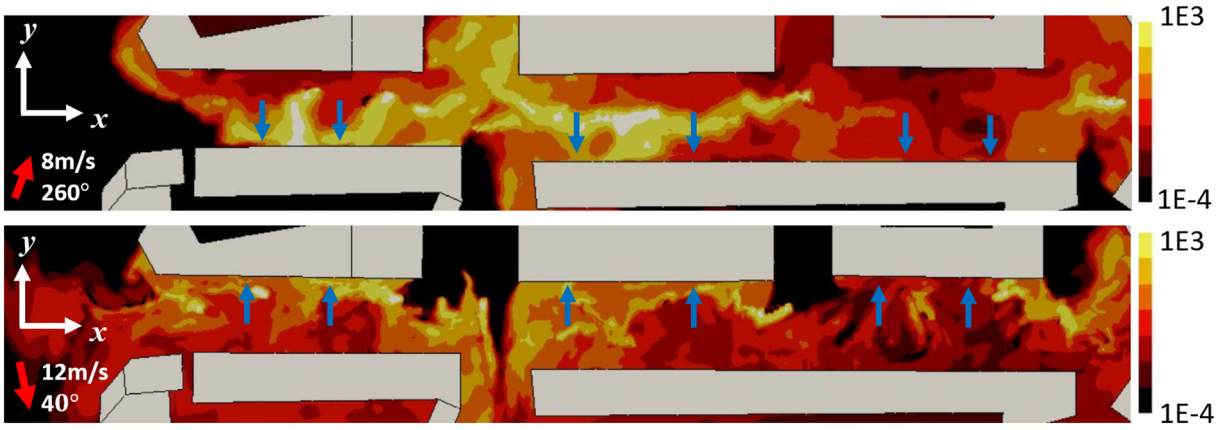

Fig. 4. Snapshot of instantaneous NO_x concentration ($\mu g.m^{-3}$) field along London Road during run 1. Red arrow shows the prevailing wind direction at the reference height of 200 m. Blue arrows indicate the prevailing wind direction at street level due to the street canyon effect.

cyclists travelling along a road with no room to filter through traffic. The mean journey time for the cyclists was 78 s with a 23 s standard deviation. For the 48 s traffic light cycle simulations 75 cyclists were simulated, while for the 96 s traffic light cycle simulations there were 64 cyclists in total. As this group of cyclists was modelled using PTV Vissim, we were not able to simulate as many as for the other two groups, nor were we able to specify the exact number.

2.2.4. Methods used to evaluate exposure

The exposure received from each pedestrian or cyclist journey was calculated using three different methods:

1. Using the concentrations resulting from the constant volume source (VS). These concentrations vary at 1 s resolution due to the wind flow and turbulence within the street; however, the emission source is constant with time.

2. Using time-averaged mean concentrations resulting from the moving tailpipe emissions. These concentrations are resolved at high spatial resolution (2 m), but are assumed constant in time for the duration of the exposure analysis and are calculated by taking the time-average mean concentration over the duration of the simulation. We refer to this method as High Spatial (HS) resolution.

3. Using the 1 s resolution concentrations resulting from the moving tailpipe emissions. These vary with time both due to the highly variable vehicle emissions and the wind flow turbulence. We refer to this method as high spatio-temporal (HST) resolution.

2.2.5. Definition of "run", "route" and "scenario"

When discussing the results below we will refer to a run (R) as a single simulation run, of which there are 4 in total (see Table 1). Between each run, the long-term mean statistics of the input data varies, i.e. either the meteorology conditions or time-averaged traffic flow rates are different.

Each run consists of multiple routes (r) for each active travel group, e.g. for pedestrians there are 4 routes (see Fig. 3). Between each route, the path taken along the road varies.

We refer to each combination of simulation run and route as a scenario, numbered $k = (1, 2, \ldots, n)$, where for pedestrians $n = 4$ runs $\times$ 4 routes = 16. So, for example, scenario $k = 1$ represents run 1 and route 1, i.e. R1r1. For each individual scenario, both the long-term statistics of the input data (i.e. meteorology and traffic inputs) and the path taken along the road are the same.

There are 800 pedestrian journeys for each simulation run, resulting in a total of 3200 pedestrian journeys across all 16 pedestrian scenarios. The total exposure, E_i, of a pedestrian for a journey, i, can be described by the sum of $\overline{E}_k$, the mean exposure of all pedestrians for any particular scenario, k, and $E'_{k,t}$ the variation about the mean for this pedestrian (Eq. (1)). The variation in journey exposure about the mean, $E'_{k,t}$, depends on the exact time of departure, t, along the street, which in turn dictates the time series of concentrations experienced by that pedestrian or cyclist. E_i can therefore be expressed as:

$$E_i = E_{k,t} = \overline{E}_k + E'_{k,t} \quad (1)$$

3. Results

3.1. Vehicle emissions along the road

Fig. 5 shows the median, mean and mean plus standard deviation of the emission rates for all traffic for each 10 m section of road length. While two different traffic configurations were used, we present the combined statistics of both here. Similarly, the analysis in the rest of the paper focuses on the statistics across all four simulation runs combined, rather than each one individually.

Fig. 5 shows that the median emission rate for all traffic is much lower than the mean for the vast majority of road length. Elevated median emissions occur near the junction and bus stops (yellow and orange shaded areas), but is otherwise very low, often close to zero, along most of the street. This is the expected behaviour as vehicle NO_x emissions tend to be dominated by short, sharp peak emissions while accelerating (O'Driscoll et al., 2016; Peckham et al., 2020), which is more likely to occur at these locations. Similarly, mean traffic emissions are elevated near these locations, in addition to the variation in emission rates represented by the standard deviation.

3.2. Pedestrian and cyclist exposures for the total journey

Table 2 shows the statistics for the mean journey concentrations, for all pedestrians and cyclists. The mean concentration calculated using the VS method underestimates that calculated using the HST methods, by 6 %, 8 % and 15 % for pedestrians, cyclists along a cycle path and cyclists along the road, respectively. The mean values calculated using the HS and HST methods are in good agreement, all within 2 %. The median value is lower for the HST method for all three groups. Similarly, the standard deviation and range of values, shown by the minimum and maximum values, are considerably greater for the HST method for each group. Therefore, while the HS method is able to estimate the mean exposure accurately, it is not able to replicate the full range of exposures experienced by individuals belonging to each group.

To understand the underlying cause of the values in Table 2, we consider the breakdown in mean journey exposures by route and by simulation run. Fig. 6 shows the range of concentrations for each scenario for pedestrians. For the HST (Fig. 6c), the variation in mean concentration between

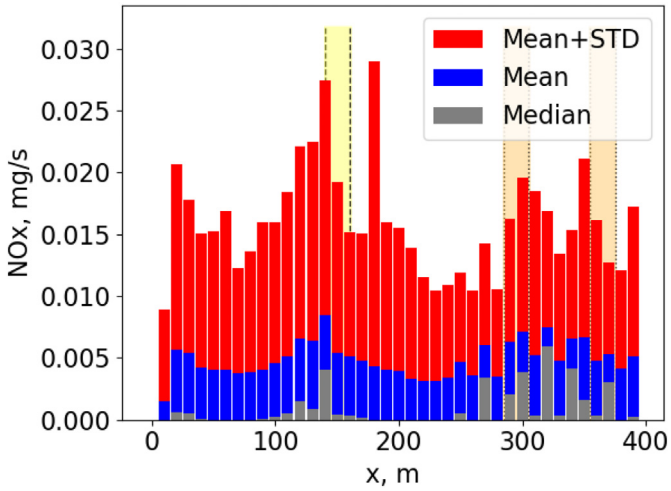

Fig. 5. Median, mean and mean plus standard deviation of 1 s vehicle emission rates for all traffic for each 10 m section of road for all simulation runs. The yellow shaded area shows the location of the pedestrian crossing, while the orange shaded areas show the location of the bus stops.

pedestrians is mostly due to a variation in concentrations within each scenario, e.g. there is a range of concentrations for the pedestrians belonging to R1r1. Here the scenario configuration is the same, i.e. the same route is taken for the same simulation run. The variation is entirely due to the *temporal* variation of concentrations along each route, leading to a variation in the term $E'_{k,t}$ in Eq. (1). It is the time of departure, t, of the pedestrian which determines the difference between the pedestrian's journey exposure, $E_{k,t}$, relative to the scenario mean, $\overline{E}_k$ – two pedestrians walking the same route at two different times will experience different concentrations as they move along the street. Only resolving at high temporal resolution can $E'_{k,t}$ be evaluated.

There is also the variation between each scenario mean $\overline{E}_k$, e.g. the difference in mean concentrations seen for R1r1 as compared to R1r2, or R2r1. This is due to the *spatial* variation in the time-averaged concentration field. This can be seen to be the case by considering Fig. 6b and c, where the values of the mean exposure (green triangles) for each scenario for the HS and HST methods are in close agreement. This again is to be expected as the time-averaged concentration field is the same in both cases. This variation *between* scenarios is significantly less than the variation *within* scenarios for the HST case. It is therefore clear that, in order to capture the full range of possible journey exposures of pedestrians walking along the street, a high temporal resolution is required for the concentrations.

For the VS case (Fig. 6a), a different pattern is seen for the scenario means as the time-averaged concentration field is not the same in this case. The variation about each scenario mean is caused by highly local dispersion patterns within the street, leading to temporal variations in concentrations despite the constant release rate.

Table 2
Mean journey NO_x concentrations ($\mu g.m^{-3}$) for pedestrians and cyclists calculated using each method; Volume Source (VS), High Spatial (HS) and High Spatio-temporal (HST). Cyclists(P) denotes cyclists travelling along the path and Cyclists (R) denotes cyclists travelling along the road.

	Pedestrians			Cyclists(P)			Cyclists(R)		
	VS	HS	HST	VS	HS	HST	VS	HS	HST
Median	16.4	18.1	16.1	23.1	26.5	19.3	23.3	28.9	20.1
Mean	16.6	17.9	17.6	23.4	25.8	25.5	23.7	31.3	31.7
Std Dev	3.6	3.5	8.3	8.2	5.7	21.0	9.3	15.8	33.5
Min	6.9	10.5	4.3	5.5	6.8	14.8	0.9	7.8	2.0
Max	29.8	25.5	82.2	47.6	42.1	196.1	48.3	112.8	283.6

A similar comparison is seen for both sets of cyclists, see Figs. S2 and S3 in the supplementary material.

3.3. Variation in exposures along the road

Fig. 7 shows the median, mean and mean plus standard deviation 1 s concentrations for all pedestrians for each 10 m section of the road. For pedestrians, the greater mean exposure estimated using the HS and HST methods is mainly due to elevated concentrations near the bus stops towards the furthest end of the road (indicated by the orange shaded areas). These elevated mean concentrations are partly a result of elevated bus emissions in these locations due to both idling emissions as buses wait for passengers to alight and board, and the emission peaks as the buses accelerate away from standstill, which contribute to the elevated emissions seen in Fig. 5. However, the peaks in pedestrian exposure are more pronounced than those in emissions. This is due to the closer proximity of the buses to pedestrians while buses wait at the bus stops (buses pull into a lay-by and are therefore a couple of metres closer to the pedestrian routes than elsewhere along the street). Passing pedestrians are therefore in closer proximity to the bus tailpipes and are exposed to higher concentration puffs when a bus pulls away and emits a short, high emission puff of NO_x.

A similar effect is not as pronounced for pedestrians near the junction (yellow shaded area), where mean concentrations are close to the mean for the entire road length (denoted by the dashed black line). This perhaps seems surprising given that most vehicles are required to stop at the junction before accelerating away, and a peak in emissions is seen at this location (Fig. 5). However, there is an opening between the buildings at both sides of the junction, which is, therefore, more exposed to wind-driven ventilation, for both modelled wind directions. A stable, higher velocity wind flow across the road is seen at the junction for both wind directions as compared with the location of the bus stops. Therefore, the puffs released by vehicles tend to be quickly dispersed and diluted, leading to a lower mean exposure than might otherwise be expected. The effect of this wind flow across the junction on concentrations can be seen in Fig. S1, where lower concentrations are seen at the location where pedestrians are crossing for both the HST (Fig. S1(a)) and VS (Fig. S1(b)) methods. These figures also show how the exposure of pedestrians at the junction is likely highly sensitive to the location of the crossing. Despite this, the elevated emissions at the junction lead to a peak in the median and mean plus standard deviation exposures.

For the cyclists travelling along a roadside path (Fig. 8) there are again elevated mean concentrations near the bus stops for the HS and HST methods, but also in this case elevated mean concentrations near the junction. These elevated mean concentrations at the junction occur because of the closer proximity of these cyclists to the vehicle tailpipes. The variation in concentrations for the HST method is greater than that for pedestrians for the majority of the road length, with the greatest variation again occurring near the junction and bus stops.

For the cyclists travelling along the road itself (Fig. 9), there are two distinct hotspots for the mean concentration, one at the junction, and another near the bus stops at $x \approx 320$ m, for both the HS and HST methods. These correspond to locations where the cyclists wait directly behind vehicles on the road before vehicles accelerate away, releasing a short, high emission puff directly into the path of the cyclist. The location of the peak for cyclists travelling along the road differs to that for cyclists travelling along the path, reflecting the different interaction with traffic between the two groups. The variation in exposures at these two locations is particularly large, and significantly greater than those seen elsewhere for each group (notice that the scale for the cyclists(R) in Fig. 9 is greater than in Figs. 7 and 8).

These results highlight the importance of the proximity of active travellers to the tailpipe. In this case, the closer proximity of the cyclists travelling along the road not only leads to a significantly greater mean journey exposure ($31.7\ \mu g.m^{-3}$) compared to the cyclists travelling along a dedicated cycle path ($25.5\ \mu g.m^{-3}$) and pedestrians ($17.6\ \mu g.m^{-3}$), but

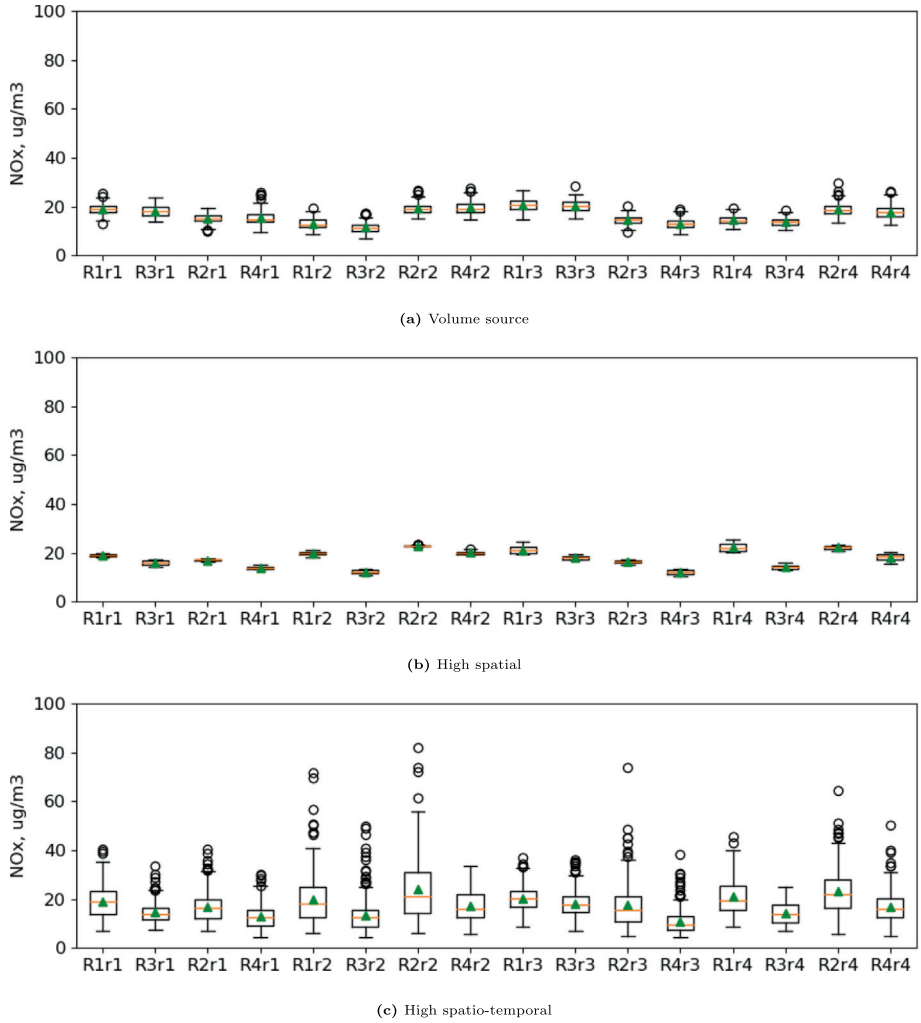

(a) Volume source

(b) High spatial

(c) High spatio-temporal

Fig. 6. Boxplots of mean journey concentrations for each run (R1, R2, R3, R4) and each pedestrian route (r1, r2, r3, r4). The green triangle denotes the mean, the orange line the median, and the box the inter-quartile range. The whiskers extend to 1.5 times the inter-quartile range.

also a much greater maximum journey exposure (283.6 $\mu g.m^{-3}$ compared to 196.1 $\mu g.m^{-3}$ and 82.2 $\mu g.m^{-3}$, respectively).

3.4. Variation in 1 s exposures

Now let us consider the variation in exposures at 1 s resolution. Fig. 10a shows the concentrations to which four pedestrians were exposed as they travelled along the road. The plots show that the concentrations can be highly variable, with significantly different profiles for each example (note that the scale of the y-axis differs between the four examples). For a large duration of the journey the concentrations are very low (<5 $\mu g.m^{-3}$), but are punctuated by very short duration, very high concentration peaks. In the second plot, concentrations above 1000 $\mu g.m^{-3}$ are seen, albeit only for a second. Fig. 10b shows the probability density function for all 1 s concentrations experienced by all pedestrians. The distribution is clearly not normal, with a mean

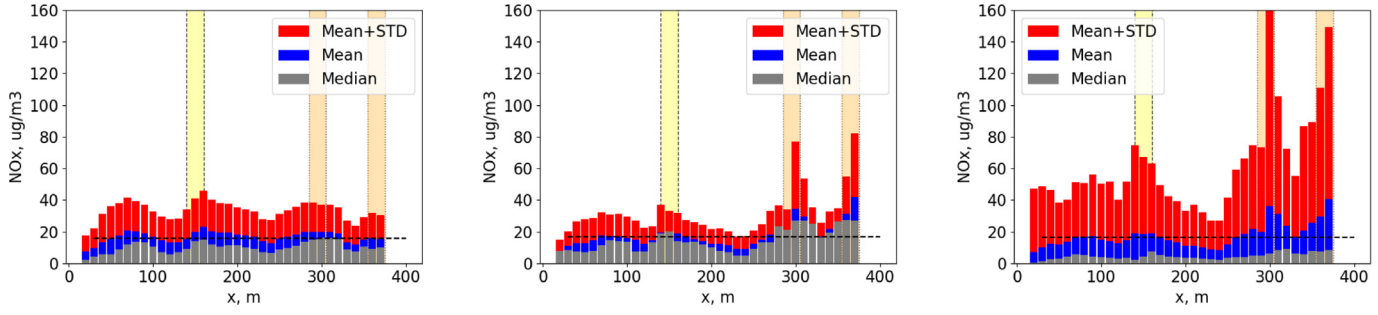

(a) Volume source (b) High spatial (c) High spatio-temporal

Fig. 7. Median, mean and mean plus standard deviation concentrations to which pedestrians are exposed for each 10 m length of road. The yellow shaded area shows the location of the pedestrian crossing, while the orange shaded areas show the location of the bus stops.

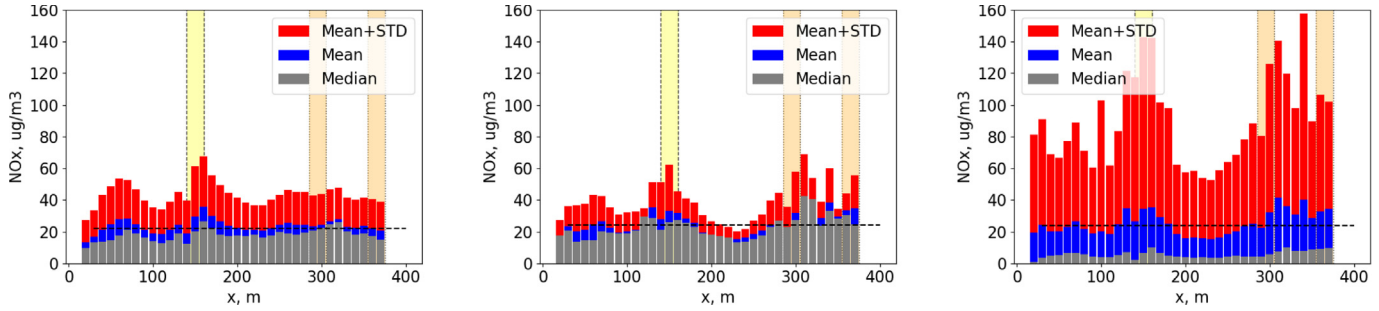

(a) Volume source (b) High spatial (c) High spatio-temporal

Fig. 8. Median, mean and mean plus standard deviation concentrations to which cyclists travelling along the roadside path (Cyclists(P)) are exposed for each 10 m length of road. The yellow shaded area shows the location of the pedestrian crossing, while the orange shaded areas show the location of the bus stops.

(17.6 $\mu g.m^{-3}$) significantly greater than the median (4.2 $\mu g.m^{-3}$) (see Table 3). There is also a large variation in concentrations about the mean, with a standard deviation of 50.9 $\mu g.m^{-3}$, and a maximum as high as 3223.0 $\mu g.m^{-3}$ (note that the x axis in the plot has been limited to 200 $\mu g.m^{-3}$). Fig. 11 shows the distributions for the VS and HS methods. It is clear that neither of these is able to accurately characterise pedestrian exposure at this time resolution as the shape of the distribution is significantly different for both cases. In the case of the HS method a bimodal distribution is seen, where the second mode is caused by the pedestrians passing through the hotspots in time average concentration at the junction or near the bus stops (Fig. S1). The shape of the VS method distribution depends entirely on the specific wind direction and street geometry and is narrower than that for the other two methods due to the constant emission source. Similar comparisons are seen for both cyclist groups.

Table 3 shows the concentration statistics calculated at 1 s resolution for all pedestrians and cyclists across all scenarios using the HST method. Also included are columns showing the values calculated excluding the 99th percentile 1 s concentrations across all scenarios. For pedestrians this equates to excluding all concentrations above 202.8 $\mu g.m^{-3}$, for cyclists(P) all concentrations above 318.9 $\mu g.m^{-3}$ and for cyclists(R) all concentrations above 363.4 $\mu g.m^{-3}$. Were these peak concentrations somehow avoidable by pedestrians and cyclists as they travelled along the road, their mean exposures would be reduced by approximately 20 % in each case. It is of course impossible for pedestrians or cyclists to detect and avoid these peak concentrations in real life. But there may be behavioural changes that could reduce the probability of exposure, such as avoiding locations where peak exposures are most likely to occur. For example, Fig. 12 shows at which distances along the length of the road these very high peak exposures tend to occur. For both pedestrians and cyclists there is a peak at the junction ($x \approx 150$ m) and near the bus stops. For pedestrians, 15 % of these peak concentrations occur within the same 10 m section of road near the junction (Fig. 12a), with an additional 26 % due to two peaks near the bus stops. For cyclists(P) the value is 15 % near the junction and 12 % near the bus stops (Fig. 12b), while for cyclists(R) it is as high as 32 % at the junction and 19 % near one of the bus stops (Fig. 12c). The peak at the junction for the pedestrians is largely due to the greater proportion of time spent at this location, shown by the black bars. However, for both cycling groups, in particular cyclists(R), the peaks are not entirely due to the greater proportion of time at this location. The peaks near the bus stops for each group occur without any significantly greater proportion of time spent at these locations.

4. Discussion

Before we discuss the results, the limitations of this study should be noted. The study considers two different wind directions only, and the boundary layer is assumed to be neutral in both cases. Two sets of traffic flows are also considered bringing the total number of simulations to four. This is obviously not a sufficient number to be able to draw general conclusions about pedestrian exposures. Further, note that no background concentration has been included in the analysis. However, these simulations do provide a test case which shows how varying model resolution even down to scales of metres and seconds can have a large impact on the characterisation of the exposure of active travellers as they move along a street in London.

Another limitation of the current work is the absence of vehicle-induced dispersion. While Fluidity is able to simulate the effect of each individual vehicle on the airflow, the method is analogous to representing the vehicle fleet as a second, highly viscous fluid (see Woodward et al., 2019), this model was not included for the current work due to the increased computational resources required. Woodward et al. (2019) showed that this effect

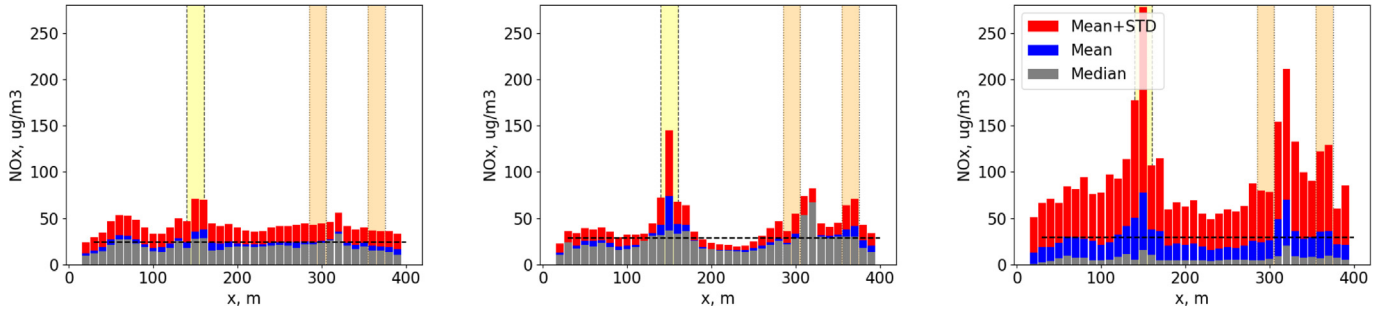

(a) Volume source (b) High spatial (c) High spatio-temporal

Fig. 9. Median, mean and mean plus standard deviation concentrations to which cyclists travelling along the road (Cyclists(R)) are exposed for each 10 m length of road. Note that the y-axis scale is greater in this case than for the corresponding figures for pedestrians and Cyclists(P). The yellow shaded area shows the location of the pedestrian crossing, while the orange shaded areas show the location of the bus stops.

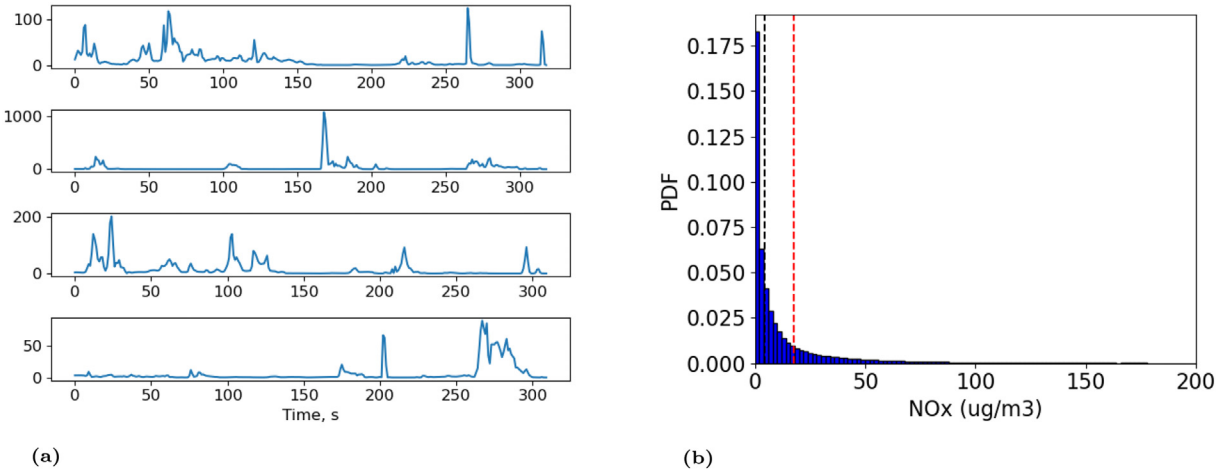

Fig. 10. (a) Time series of NO_x concentration exposure ($\mu g.m^{-3}$) for four pedestrians taking route 1, 2, 3 and 4 from top to bottom. Concentrations shown are for simulation run 1. Note the different y-axis scales for each example. (b) HST method probability density function for all NO_x concentrations experienced by the simulated pedestrians for all routes and all simulation runs. The black dashed line indicates the median (4.2 $\mu g.m^{-3}$) and the red dashed line the mean (17.6 $\mu g.m^{-3}$). The x axis has been limited to 200 $\mu g.m^{-3}$, though concentrations go up to a maximum of 3223.0 $\mu g.m^{-3}$.

Table 3
Pedestrian and cyclist statistics calculated at 1 s resolution for all scenarios using the High Spatio-temporal (HST) method. Cyclists(P) denotes cyclists travelling along the path and Cyclists(R) denotes cyclists travelling along the road.

	Ped.	Excl. 99th %ile	Cyclists (P)	Excl. 99th %ile	Cyclists (R)	Excl. 99th %ile
Median	4.2	4.1	5.1	5.0	6.1	5.9
Mean	17.6	13.9	25.6	20.4	31.8	25.6
Std Dev	50.9	24.5	71.8	41.0	85.1	49.3
99th %ile Max	202.8	133.0	318.9	220.2	363.4	257.1
	3223.0	202.8	3600.5	318.9	2150.0	363.3

can have a significant impact on street-level concentrations; vehicle movement drags pollutants along the street and dilutes them through wake turbulence, extending regions of high concentration but reducing peak levels.

4.1. Possible implications for pedestrians and cyclists

Comparing the 1 s resolution statistics for pedestrians and the two cycling groups seen in Table 3, we see that the median is similar across all groups. This is despite the closer proximity of the cyclists to the road than pedestrians, in particular the cyclists travelling along the road itself, rather than the path, which are often very close to vehicle tailpipes. The median is by definition the 50th percentile of the 1 s concentrations experienced by each group. Given that the median concentrations are fairly low ($\leq$6.1 $\mu g.m^{-3}$), this means that the concentrations experienced by each group is very similar for at least half the time. In fact, we find that the 1 s concentrations experienced by pedestrians are below the mean value of 17.6 $\mu g.m^{-3}$ for 78 % of the time. For cyclists(P) the concentration is below 17.6 $\mu g.m^{-3}$ for 74 %, and for cyclists(R) for 70 % of the time. This is true despite significant differences in the mean concentrations experienced by each group, with the mean for cyclists on the road being 80 % greater than that for pedestrians, and 24 % greater than that for the cyclists on the path. The reason for the difference in the time-average mean, and the key difference between the exposure of each group, is the magnitude and

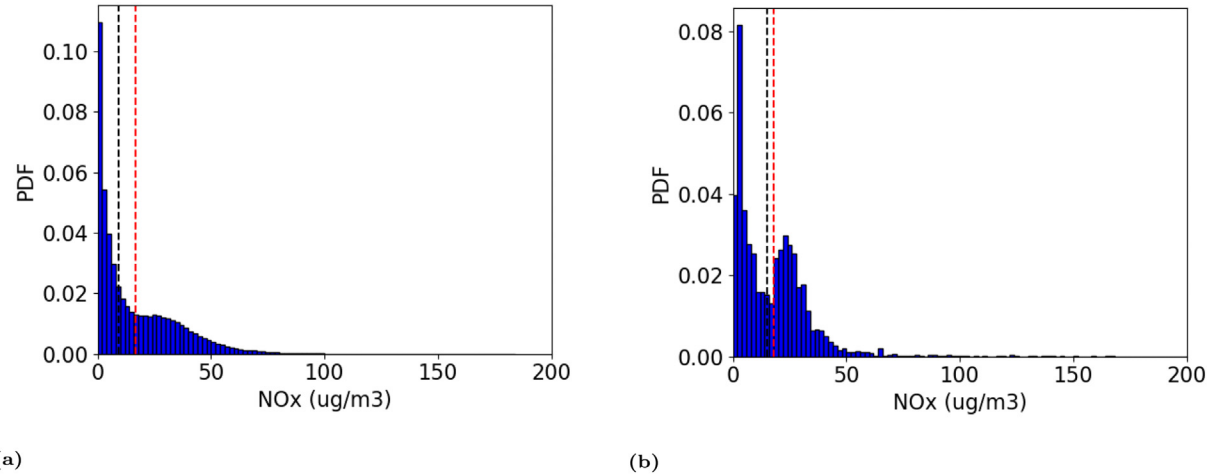

Fig. 11. (a) VS method probability density function for all NO_x concentrations experienced by the simulated pedestrians for all routes and all simulation runs. The black dashed line indicates the median (9.4 $\mu g.m^{-3}$) and the red dashed line the mean (16.6 $\mu g.m^{-3}$). The maximum concentration is 183.5 $\mu g.m^{-3}$. (b) HS method probability density function for all NO_x concentrations experienced by the simulated pedestrians for all routes and all simulation runs. The black dashed line indicates the median (15.0 $\mu g.m^{-3}$) and the red dashed line the mean (17.9 $\mu g.m^{-3}$). The x axis has been limited to 200 $\mu g.m^{-3}$, however concentrations go up to a maximum of 215.2 $\mu g.m^{-3}$.

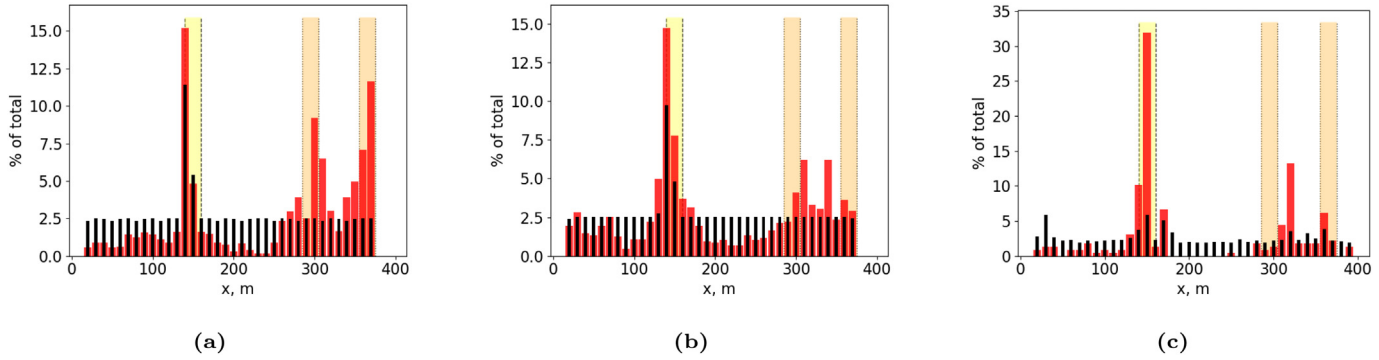

Fig. 12. Percentage of 1 s 99th percentile exposures that occur (red) and percentage of total time spent (black) at each 10 m section of road for a (a) pedestrian, (b) cyclists travelling along the path (cyclists(P)) and cyclists travelling along the road (cyclists(R)). The yellow shaded area shows the location of the pedestrian crossing, while the orange shaded areas show the location of the bus stops.

frequency of exposure to the very short, high concentrations, such as those seen in Fig. 10a. Reducing the likelihood of exposure to these peak concentrations could lead to significant reductions in mean exposures. For the scenarios considered in this study, avoiding the 99th percentile concentrations results in a reduction in mean exposure of 3.7 $\mu g.m^{-3}$ for pedestrians, 5.2 $\mu g.m^{-3}$ for cyclists on the path and 6.2 $\mu g.m^{-3}$ for cyclists on the road.

A measure that could achieve this for cyclists would be to locate cycle lanes away from busy roads. In fact, the results presented here suggest that even a cycle path directly next to the road can reduce exposures significantly. Failing this, a secondary measure could be to ensure that there is space for cyclists to filter through traffic rather than having to stop and wait among vehicles.

For pedestrians, measures could target the peak exposures seen at the junction and bus stops. Although only four simulations are considered here, we can say with confidence that busy junctions and bus stops are locations with greater statistical probability of being emission hotspots, and where peak emissions such as those seen by O'Driscoll et al. (2016) and Peckham et al. (2020) are likely to occur. In which direction these emission peaks are dispersed will depend on the meteorology at the time, however exposure to these peak concentrations is still statistically much more likely in these areas than elsewhere on the street. These locations also tend to be where pedestrians spend a disproportionate amount of time, therefore enhancing the impact of these peak exposure rates. Even for our simulations where pedestrians waiting for buses was not considered, all pedestrians walked past the bus stops without stopping, these locations contributed disproportionately to the total journey exposures. Placing bus stop queues further from the road could be an effective option, another to design bus stops that provide shelter for pedestrians from these high concentration puffs.

Future work will attempt to evaluate the relative importance of the time required by pedestrians to wait at the junction to total exposure, in addition to the effect of waiting at the bus stops. Additional meteorological conditions will also be investigated, including low wind speed conditions.

4.2. The suitability of mean concentrations for health impact assessment

The nature of exposure at high resolution shown here raises the question as to whether the mean concentration is a suitable value when attempting to quantify the harm caused by chronic exposure to NO_x/NO_2, and whether the variation in concentrations experienced by individuals along the road holds any significance when evaluating the impact of exposure on health. Both epidemiological studies and controlled clinical studies of the harm caused by exposure to NO_2 tend to use the time-averaged mean concentration as the variable quantifying the magnitude of exposure (World Health Organization, 2010). Assuming a linear function of the time-averaged concentration is equivalent to assuming that Haber's law for toxicity (Haber, 1924) holds for NO_2. Haber's law states that the incidence or severity of a toxic effect depends on the time integral of the concentration over the period of exposure T, $\int_0^T C(t)dt$, or equivalently a linear function of the time-average mean concentration and time of exposure, $\bar{C} \times T$. This is done despite an extensive literature suggesting that Haber's law does not typically hold for inhaled toxicants, including NO_2 (e.g. Jarabek, 1995; Miller et al., 2000; Bunce and Remillard, 2003), at least for short-term, acute exposures. Rozman and Doull (2000) hypothesise that a deviation from Haber's law occurs when a steady-state or equilibrium state is prevented from being reached by an intermittent or variable dose, i.e. a highly variable dose leads to a nonlinear toxic response when described as a function of the time-averaged mean concentration. Animal experiments which have compared continuous and intermittent exposures suggest that a nonlinear function is a more accurate model for the toxicity of NO_2 (Gardner et al., 1979; Rombout et al., 1986; ten Berge et al., 1986). It should however be noted that these experiments involve much higher concentrations than those seen at the roadside and that concentration-time functions derived for short-term, acute exposures may not translate to long-term, chronic exposure.

Epidemiological population or cohort studies tend to use linear models of time-average mean concentrations to derive concentration response functions for chronic NO_2 exposure. Studies of all-cause and respiratory mortality which have given specific consideration to the shape of the concentration response function have in the most part concluded that they do not significantly deviate from linearity (Cesaroni et al., 2013; Fischer et al., 2015; COMEAP, 2018). However, there exists a substantial heterogeneity in the response functions derived from different studies (COMEAP, 2018). In a recent review, Huangfu and Atkinson (2020) concluded that the evidence does not currently exist to determine the precise nature (magnitude and linearity) of mortality associations with long term, time-averaged mean NO_2 exposure. Further, despite the general acceptance of linearity in most cases, there is evidence of nonlinearity at low concentrations with several studies reporting a steeper response function (i.e. more harm caused for each increment of concentration increase) below a certain threshold effect (typically <20 $\mu g.m^{-3}$) (Næss et al., 2006; Crouse et al., 2015; Halonen et al., 2016). Halonen et al. (2016) looked specifically at traffic emissions in London and found that the all-cause and cardiovascular mortality concentration response functions were nonlinear, however the positive association between exposure and mortality was weak.

Given the highly complex and transient nature of the numerous processes that occur when a toxicant is inhaled and then causes harm, the transient toxicant elimination then recovery processes which follows exposure, and the highly varying concentrations experienced by exposed individuals, it seems unlikely that Haber's rule will hold for NO_2 exposure near a roadside. Rather, it seems likely that a nonlinear relationship between harm and exposure is more appropriate, i.e. $\int C(t)^n dt$, where $n \neq 1$. While the evidence and understanding certainly does not yet exist to justify a move

away from the use of Haber's law to quantify the degree of harm caused by chronic exposure to NO_2, a greater understanding of the variation in exposure about the mean can only help improve our understanding of the mechanism of harm. The availability of concentration data with fine time and spatial resolution opens up the possibility of developing dynamical models for exposure that include physiological processes, recovery, etc.; for an example, see Hilderman et al. (1999).

The total harm incurred from exposure depends on the form of the exposure-harm-recovery relationship, which need not be linear. The question then arises as to which statistic or function of the concentration time series encountered by an individual is most appropriate in determining the harm caused over any period of time or, in this case, journey along London Road. Possible answers might include the mean, the median or a measure of the extreme, such as the 95th percentile - or, perhaps, only the actual concentration time series. We note that the mean is the appropriate measure only if the exposure-response function is linear. This is no longer true if the exposure-response function is nonlinear.

Some aspects of harm and exposure under a nonlinear regime are worth noting. First, consider a nonlinear exposure-response function without a threshold, with the effective harm given by $D = \int_0^T C(t)^n dt$, T being the duration of exposure. The peaks in the concentration time series acquire ever greater significance as n increases above unity and, as previously noted, $n>1$ has been argued for a number of common pollutants. However, n will generally have been determined from exposure to increasing levels of steady concentration, and it is not clear that this necessarily provides a reliable value to be used with sporadic exposure. Second, consider a nonlinear response function above a threshold, C_{th}, so that only times when $C(t)>C_{th}$ contribute to D. Situations can now occur where the mean and median are below the threshold, but the peaks exceed it. In all of these circumstances, use of the time series, $C(t)$, would appear to be obligatory in the absence of a model which can give representative predictions of the required statistics, e.g. number and magnitude of C_{th} exceedances.

4.3. Possible implications for modelling exposure

In Section 3.2 we found that the mean exposure of pedestrians and cyclists travelling along the road was in good agreement between the high spatial and high spatio-temporal resolution cases. While the volume source method provided a reasonable estimate of the pedestrian mean exposure, it significantly underestimated the mean exposure of cyclists, mainly due to the fact that the volume source method did not capture localised concentration hotspots near the junction and bus stops where emissions tend to be greatest. This suggests that a high spatial resolution is sufficient to estimate mean exposures, without requiring a comparable degree of temporal resolution. However, the high spatio-temporal method showed that there is a considerable degree of variation in possible exposures for both pedestrians and cyclists about the mean which was not fully captured by the volume source and high spatial methods. While the high spatial method is able to capture the spatial variation in exposures due to changes to longer term statistics, e.g. the different time-averaged concentration field for different routes, or different traffic configurations or wind directions, it is not able to capture the large variation in journey exposures due to the high degree of temporal variability in concentrations over time periods down to 1 s. For the high spatial-temporal method an order-of-magnitude variation was seen in the time-average mean exposure of pedestrians (4.3–82.2 $\mu g.m^{-3}$) and for cyclists along a path (14.8–196.1 $\mu g.m^{-3}$), and two orders of magnitude for cyclists along a road (2.0–283.6 $\mu g.m^{-3}$). Therefore, the highly variable 1 s resolution concentrations experienced by pedestrians translates to significant variations in exposure over longer time periods (the mean journey time for pedestrians was over 5 min).

It is of course important to note that these exposures consider only the traffic emissions along the simulated road. In reality, concentrations will be elevated by contributions from emissions in the surrounding area and therefore these ranges will be less significant relative to the mean. However, analysis of NO_2 concentrations measured at 1 s time steps on the roof of a car driving along London roads, over the course of two days, also show a mean significantly higher than the median, and a distribution that is log normal (see Figs. S4 and S5 in supplementary material). These measurements were taken as part of the Breathe London project (Breathe London Pilot, n.d.). It therefore seems that only by resolving to time scales down to the breathing cycle can the exposure of pedestrians and cyclists travelling through urban areas be fully and accurately characterised.

While the exposures considered here are representative of periods of travel activity which make up only a small proportion of people's day, such activities can represent as much as a quarter of air pollution intake in daily lives (de Nazelle et al., 2013).

5. Conclusion

The exposure of a group of pedestrians and two groups of cyclists, one travelling along a roadside path and another along the road itself, was simulated using a high spatio-temporal model of NO_x concentrations and a simple agent-based simulation. A road in London was used as a test case and four simulations were run in total with two wind directions and two traffic configurations. A comparison was made between the exposure of the different active travel groups using different methods to simulate the NO_x concentrations.

It was shown that in order to characterise pedestrian and cyclist exposures realistically, a high spatial and temporal resolution model was required, with time resolution down to the timescale of the breathing cycle ($\approx$ 1 s). Use of a high spatial resolution model with constant concentrations in time provided good estimates of mean exposure but failed to replicate the range of exposures encountered by individual pedestrians and cyclists. This variation was large when evaluated using the high spatio-temporal resolution method, with an order of magnitude or greater variation in possible time-average mean exposures depending on the time of departure along the street. This showed that resolving the concentration field down to 1 s leads to significant variations in exposure over longer time periods, in this case the time taken to travel the length of the road (for pedestrians just over 5 min).

We also found that pedestrian and cyclist exposures were dominated by short, very high peak, localised exposures. The majority of these occurred either at the junction or near the bus stops in the study area. It is at these locations where vehicles are required to accelerate from standstill, often emitting a large spike of NO_x as they do so. This emission behaviour is well understood and therefore it is likely that we already know where the key hotspots are along any street. It may therefore be possible to reduce the exposure of active travellers using measures targeted at these locations, for example maximising the distance between pedestrian crossings and the stop line for vehicles or building cycling infrastructure away from the road.

These acute exposures lead to a log normal distribution in 1 s resolution exposures, with mean concentrations experienced significantly greater than the median. The 1 s resolution concentrations experienced by the pedestrians and cyclists modelled in these case studies were below the mean for the vast majority of the time (78 % of the time for pedestrians). This raises the question as to how suitable the use of the time-average mean concentrations is when evaluating the impact of exposure on health; the mean captures neither the concentration experienced for the majority of the time spent at the roadside, nor the number and magnitude of peak exposures. Further, given the highly variable concentrations when considered at the breathing time scale and the complex and transient nature of exposure-harm-recovery processes, we question whether Haber's rule should be assumed to hold for NO_2 exposure near a roadside.

A better characterisation of the exposure is likely required in order to improve our understanding of the mechanism of harm from chronic exposure to NO_2, and other highly variable pollutants in urban areas.

Funding

This work was funded by the Engineering and Physical Sciences Research Council (EPSRC) Grand Challenge grant 'Managing Air for Green Inner Cities (MAGIC) [grant number EP/N010221/1].

CRediT authorship contribution statement

H Woodward: conceptualisation, methodology, software, formal analysis, data curation, writing – original draft, visualisation. **A Schroeder:** conceptualisation, writing – original draft. **A de Nazelle:** writing – original draft, supervision, funding acquisition. **C C Pain:** methodology, funding acquisition. **M E J Stettler:** conceptualisation, methodology. **H ApSimon:** supervision, funding acquisition. **A Robins:** writing – original draft, funding acquisition. **P F Linden:** writing – original draft, funding acquisition.

Data availability

Data will be made available on request.

Declaration of competing interest

The authors declare that they have no known competing financial interests or personal relationships that could have appeared to influence the work reported in this paper.

Appendix A. Supplementary data

Supplementary data to this article can be found online at https://doi.org/10.1016/j.scitotenv.2023.163711.

References

Aristodemou, E., Boganegra, L.M., Mottet, L., Pavlidis, D., Constantinou, A., Pain, C.C., Robins, A., ApSimon, H., 2018. How tall buildings affect turbulent air flows and dispersion of pollution within a neighbourhood. Environ. Pollut. 233, 782–796. https://doi.org/10.1016/j.envpol.2017.10.041.

Beevers, S.D., Kitwiroon, N., Williams, M.L., Carslaw, D.C., 2012. One way coupling of CMAQ and a road source dispersion model for fine scale air pollution predictions. Atmos. Environ. 59, 47–58. https://doi.org/10.1016/j.atmosenv.2012.05.034.

ten Berge, W.F., Zwart, A., Appelman, L.M., 1986. Concentration—time mortality response relationship of irritant and systemically acting vapours and gases. J. Hazard. Mater. 13 (3), 301–309. https://doi.org/10.1016/0304-3894(86)85003-8.

Breathe London Pilot, Breathe London Mobile https://openaq.org/#/location/61488 Online; accessed 01-May-2022.

Bunce, N.J., Remillard, R.B.J., 2003. Haber's rule: the search for quantitative relationships in toxicology. Hum.Ecol.Risk Assess. 9 (4), 973–985.. https://doi.org/10.1080/713610018.

Cesaroni, G., Badaloni, C., Gariazzo, C., Stafoggia, M., Sozzi, R., Davoli, M., Forastiere, F., 2013. Long-term exposure to urban air pollution and mortality in a cohort of more than a million adults in Rome. Environ. Health Perspect. 121 (3), 324–331. https://doi.org/10.1289/ehp.1205862.

COMEAP, 2018. Associations of Long-term Average Concentrations of Nitrogen Dioxide With Mortality. Technical Report. Committee on the Medical Effects of Air Pollutants.

Crouse, D.L., Peters, P.A., Hystad, P., Brook, J.R., van Donkelaar, A., Martin, R.V., Villeneuve, P.J., Jerrett, M., Goldberg, M.S., Arden Pope III, C., Brauer III, M., Brook III, R.D., Robichaud III, A., Menard III, R., Burnett III, R.T., 2015. Ambient PM2.5, O3, and NO2 exposures and associations with mortality over 16 years of follow-up in the Canadian census health and environment cohort (CANCHEC). Environ. Health Perspect. 123 (11), 1180–1186. https://doi.org/10.1289/ehp.1409276.

Fischer, P.H., Marra, M., Ameling, C.B., Hoek, G., Beelen, R., de Hoogh, K., Breugelmans, O., Kruize, H., Janssen, N.A.H., Houthuijs, D., 2015. Air pollution and mortality in seven million adults: the Dutch Environmental Longitudinal Study (DUELS). Environ. Health Perspect. 123 (7), 697–704. https://doi.org/10.1289/ehp.1408254.

Gardner, D.E., Miller, F.J., Blommer, E.J., Coffin, D.L., 1979. Influence of exposure mode on the toxicity of NO_2. Environ. Health Perspect. 30, 123–129. https://doi.org/10.1289/ehp.793023.

Haber, F., 1924. Zur Geschichte des Gaskrieges. Springer Berlin Heidelberg, Berlin, Heidelberg, pp. 76–92.

Halonen, J.I., Blangiardo, M., Toledano, M.B., Fecht, D., Gulliver, J., Ghosh, R., Anderson, H.R., Beevers, S.D., Dajnak, D., Kelly, F.J., Wilkinson, P., Tonne, C., 2016. Is long-term exposure to traffic pollution associated with mortality? A small-area study in London. Environ. Pollut. 208, 25–32. https://doi.org/10.1016/j.envpol.2015.06.036 Special Issue: Urban Health and Wellbeing.

Hilderman, T.L., Hrudey, S.E., Wilson, D.J., 1999. A model for effective toxic load from fluctuating gas concentrations. J. Hazard. Mater. 64 (2), 115–134.. https://doi.org/10.1016/S0304-3894(98)00247-7.

Huangfu, P., Atkinson, R., 2020. Long-term exposure to NO_2 and O_3 and all-cause and respiratory mortality: a systematic review and meta-analysis. Environ. Int. 144, 105998. https://doi.org/10.1016/j.envint.2020.105998.

Irwin, M., Bradley, H., Duckhouse, M., Hammond, M., Peckham, M.S., 2018. High spatiotemporal resolution pollutant measurements of on-board vehicle emissions using ultrafast response gas analyzers. Atmos. Meas. Tech. 11 (6), 3559–3567. https://doi.org/10.5194/amt-11-3559-2018.

Jarabek, A.M., 1995. Consideration of temporal toxicity challenges current default assumptions. Inhal. Toxicol. 7 (6), 927–946. https://doi.org/10.3109/08958379509012801.

Le Cornec, C.M.A., Molden, M., van Reeuwijk, M., Stettler, M.E.J., 2020. Modelling of instantaneous emissions from diesel vehicles with a special focus on NO_x: insights from machine learning techniques. Sci. Total Environ. 737, 139625. https://doi.org/10.1016/j.scitotenv.2020.139625.

Miller, F.J., Schlosser, P.M., Janszen, D.B., 2000. Haber's rule: a special case in a family of curves relating concentration and duration of exposure to a fixed level of response for a given endpoint. Toxicology 149 (1), 21–34. https://doi.org/10.1016/S0300-483X(00)00229-8.

Næss, Ø., Nafstad, P., Aamodt, G., Claussen, B., Rosland, P., 2006. Relation between concentration of air pollution and cause-specific mortality: four-year exposures to nitrogen dioxide and particulate matter pollutants in 470 neighborhoods in Oslo, Norway. Am. J. Epidemiol. 165 (4), 435–443. https://doi.org/10.1093/aje/kwk016 11.

de Nazelle, A., Seto, E., Donaire-Gonzalez, D., Mendez, M., Matamala, J., Nieuwenhuijsen, M.J., Jerrett, M., 2013. Improving estimates of air pollution exposure through ubiquitous sensing technologies. Environ. Pollut. 176, 92–99. https://doi.org/10.1016/j.envpol.2012.12.032.

O'Driscoll, R., ApSimon, H.M., Oxley, T., Molden, N., Stettler, M.E.J., Thiyagarajah, A., 2016. A portable emissions measurement system (PEMS) study of NO_x and primary NO_2 emissions from Euro 6 diesel passenger cars and comparison with COPERT emission factors. Atmos. Environ. 145, 81–91. https://doi.org/10.1016/j.atmosenv.2016.09.021.

Pain, C.C., Umpleby, A.P., de Oliveira, C.R.E., Goddard, A.J.H., 2001. Tetrahedral mesh optimisation and adaptivity for steady-state and transient finite element calculations. Comput. Methods Appl. Mech. Eng. 190 (29), 3771–3796. https://doi.org/10.1016/S0045-7825(00)00294-2.

Pavlidis, D., Gorman, G.J., Gones, J.L.M.A., Pain, C.C., ApSimon, H., 2010. Synthetic-eddy method for urban atmospheric flow modelling. Bound.-Layer Meteorol. 136, 285–299. https://doi.org/10.1007/s10546-010-9508-x.

Peckham, M., Parnell, J., Hammond, M., Mason, B., 2020. The measurement of fast transient emissions during real world driving. Front. Mech. Eng. 6. https://doi.org/10.3389/fmech.2020.00019.

PTV Vissim, https://www.ptvgroup.com/en/solutions/products/ptv-vissim/ Accessed: 21-03-2022.

Rombout, P.J.A., Dormans, J.A.M.A., Marra, M., van Esch, G.J., 1986. Influence of exposure regimen on nitrogen dioxide-induced morphological changes in the rat lung. Environ. Res. 41 (2), 466–480. https://doi.org/10.1016/S0013-9351(86)80141-4.

Rozman, K.K., 2000. The role of time in toxicology or Haber's c×t product. Toxicology 149 (1), 35–42. https://doi.org/10.1016/S0300-483X(00)00230-4.

Rozman, K.K., Doull, J., 2000. Dose and time as variables of toxicity. Toxicology 144 (1), 169–178.. https://doi.org/10.1016/S0300-483X(99)00204-8.

Santiago, J.L., Borge, R., Sanchez, B., Quaassdorff, C., de la Paz, D., Martilli, A., Rivas, E., Martín, F., 2021. Estimates of pedestrian exposure to atmospheric pollution using high-resolution modelling in a real traffic hot-spot. Sci. Total Environ. 755, 142475. https://doi.org/10.1016/j.scitotenv.2020.142475.

Santiago, J.L., Rivas, E., Gamarra, A.R., Vivanco, M.G., Buccolieri, R., Martilli, A., Lechón, Y., Martín, F., 2022. Estimates of population exposure to atmospheric pollution and health-related externali ties in a real city: the impact of spatial resolution on the accuracy of results. Sci. Total Environ. 819, 152062. https://doi.org/10.1016/j.scitotenv.2021.152062.

Woodward, H., Stettler, M.E.J., Pavlidis, D., Aristodemou, E., ApSimon, H., Pain, C.C., 2019. A large eddy simulation of the dispersion of traffic emissions by moving vehicles at an intersection. Atmos. Environ. 215, 116891. https://doi.org/10.1016/j.atmosenv.2019.116891.

Woodward, H., Schroeder, A.K., Le Cornec, C.M.A., Stettler, M.E.J., ApSimon, H., Robins, A., Pain, C., Linden, P.F., 2022. High resolution modelling of traffic emissions using the large eddy simulation code Fluidity. Atmosphere 13 (8). https://doi.org/10.3390/atmos13081203.

World Health Organization, 2010. WHO Guidelines for Indoor Air Quality: Selected Pollutants.